Title

Relative transmembrane segment rearrangements during BK channel activation resolved by structurally assigned fluorophore-quencher pairing.

Journal

The Journal of general physiology, 140(2)

ISSN

0022-1295

Authors

Pantazis, Antonios
Olcese, Riccardo

Publication Date

2012-08-01

DOI

10.1085/jgp.201210807

Peer reviewed

Relative transmembrane segment rearrangements during BK channel activation resolved by structurally assigned fluorophore–quencher pairing

Antonios Pantazis,[1] and Riccardo Olcese[1,2,3]

[1]Department of Anesthesiology, Division of Molecular Medicine, [2]Brain Research Institute, and [3]Cardiovascular Research Laboratories, David Geffen School of Medicine, University of California, Los Angeles, Los Angeles, CA 90075

Voltage-activated proteins can sense, and respond to, changes in the electric field pervading the cell membrane by virtue of a transmembrane helix bundle, the voltage-sensing domain (VSD). Canonical VSDs consist of four transmembrane helices (S1–S4) of which S4 is considered a principal component because it possesses charged residues immersed in the electric field. Membrane depolarization compels the charges, and by extension S4, to rearrange with respect to the field. The VSD of large-conductance voltage- and Ca-activated K^+ (BK) channels exhibits two salient inconsistencies from the canonical VSD model: (1) the BK channel VSD possesses an additional nonconserved transmembrane helix (S0); and (2) it exhibits a "decentralized" distribution of voltage-sensing charges, in helices S2 and S3, in addition to S4. Considering these unique features, the voltage-dependent rearrangements of the BK VSD could differ significantly from the standard model of VSD operation. To understand the mode of operation of this unique VSD, we have optically tracked the relative motions of the BK VSD transmembrane helices during activation, by manipulating the quenching environment of site-directed fluorescent labels with native and introduced Trp residues. Having previously reported that S0 and S4 diverge during activation, in this work we demonstrate that S4 also diverges from S1 and S2, whereas S2, compelled by its voltage-sensing charged residues, moves closer to S1. This information contributes spatial constraints for understanding the BK channel voltage-sensing process, revealing the structural rearrangements in a non-canonical VSD.

The Journal of General Physiology

INTRODUCTION

Large-conductance voltage- and Ca-activated K^+ (BK) channels are potent regulators of excitability, broadly expressed in most mammalian cells (Toro et al., 1998; Latorre and Brauchi, 2006; Salkoff et al., 2006). BK channels are formed by α-subunit homotetramers (Shen et al., 1994) (Fig. 1), each comprising a conserved transmembrane voltage-sensing domain (VSD), helices contributing to the ion-conducting pore domain, and large intracellular ligand-binding domains that assemble into the gating ring superstructure in the tetramer (Wang and Sigworth, 2009; Wu et al., 2010; Yuan et al., 2010, 2012; Javaherian et al., 2011). BK channels exhibit an exceptionally high, selective conductance for K^+, which is over an order of magnitude greater than that of other voltage-gated K^+ channels (Latorre and Miller, 1983), and their activation is regulated by the synergistic action of membrane depolarization and intracellular Ca binding (Stefani et al., 1997; Cui and Aldrich, 2000; Rothberg and Magleby, 2000; Horrigan and Aldrich, 2002; Magleby, 2003; Latorre and Brauchi, 2006; Sweet and Cox, 2008; Cui et al., 2009; Latorre et al., 2010; Lee and Cui, 2010; Savalli et al., 2012). Ca is thought to bind with high affinity to the cytosolic domain (Wei et al., 1994; Schreiber and Salkoff, 1997; Bian et al., 2001; Xia et al., 2002; Bao et al., 2004; Zeng et al., 2005; Yusifov et al., 2008, 2010; Yuan et al., 2010, 2012; Zhang et al., 2010; Javaherian et al., 2011), which is also sensitive to other ligands and biological partners that modulate channel activation (Lu et al., 2006; Hou et al., 2009).

Typical voltage-gated K^+ channel α subunits possess six transmembrane helices; the four most N-terminal helical transmembrane segments (S1–S4) comprise the VSD, whereas S5 and S6 contribute to the central ion-selective pore (Armstrong, 2003; Swartz, 2004; Long et al., 2005, 2007). Of the four conserved VSD helices, S4 is considered the principal component of voltage sensing because it has been found to concentrate most voltage-sensing charged residues, which are immersed in the electric field pervading the cell membrane and compel the helix to adopt an active conformation upon membrane depolarization (Tombola et al., 2006; Bezanilla, 2008; Chanda and Bezanilla, 2008; Swartz, 2008).

In contrast, BK channels exhibit a decentralized distribution of voltage-sensing charged residues, whereby

Correspondence to Riccardo Olcese: rolcese@ucla.edu

Abbreviations used in this paper: BK, large-conductance voltage- and Ca-activated K^+; TMRM, tetramethylrhodamine-5′-maleimide; VSD, voltage-sensing domain; WT, wild type.

The Rockefeller University Press $30.00
J. Gen. Physiol. Vol. 140 No. 2 207–218
www.jgp.org/cgi/doi/10.1085/jgp.201210807

most voltage-sensing charge is contributed from segments S2 and S3 (Ma et al., 2006). Specifically, S2 carries two voltage-sensing residues, D153 and R167; S3 bears D186, and S4 only contributes R213 (Ma et al., 2006) (Fig. 1 A). We recently showed that the charged residues borne by S2 confer intrinsic voltage-sensing properties to the S2 helix, causing it to rearrange with respect to the electric field upon depolarization, a process that results in a unique mode of intra-subunit cooperativity between S2 and S4 that could involve electric field focusing by dynamic (state-dependent) water-filled crevice formation (Pantazis et al., 2010a).

Furthermore, BK α subunits possess a distinct transmembrane topology. In addition to broadly conserved helices S1–S6, BK channels have additional transmembrane helix S0 (Wallner et al., 1996; Meera et al., 1997), which is involved in the association of auxiliary β subunits (Wallner et al., 1996; Morrow et al., 2006; Liu et al., 2008, 2010; Wu et al., 2009) and could be directly involved in the BK voltage-sensing process (Koval et al., 2007). The position of S0 with respect to other VSD and pore helices has been inferred by investigating disulfide cross-linking efficiency by Liu et al. (2010) (Fig. 1 D). The close proximity of S0 and S4 was further supported by the identification of a Trp side chain in S4 as the collisional quencher of fluorophores labeling the extracellular flank of S0 (Pantazis et al., 2010b).

Given these salient structural and functional features of the BK VSD, it is likely that BK channels use a distinct mode of sensing the membrane potential. How does S4 rearrange with respect to other VSD helices during activation? As S2 exhibits intrinsic voltage dependence, what is the direction of its depolarization-induced motion? We sought to understand how BK channels sense, and respond to, changes in the membrane potential by optically tracking voltage-dependent rearrangements using voltage-clamp fluorometry. The latter involves labeling unique cysteines introduced at specific protein positions with small thiol-reactive, environment-sensitive fluorophores (Mannuzzu et al., 1996; Cha and Bezanilla, 1997; Claydon and Fedida, 2007; Gandhi and Olcese, 2008). In addition, we exploited the photochemical properties of the tryptophan side chain, which can quench the fluorescence of small organic dyes by photo-induced e^- transfer upon van der Waals collision (Mansoor et al., 2002, 2010; Doose et al., 2005, 2009; Islas and Zagotta, 2006; Pantazis et al., 2010b) to gain structural insight to the source of the observed fluorescence deflections. Thus, we combined site-directed fluorescent labeling under voltage clamp with manipulation of fluorescence quenching by the removal of a native Trp, or the strategic introduction of additional Trp residues, to reveal the relative voltage-dependent rearrangements of assigned protein positions. We found that the extracellular portion of S4 diverges from S1 upon VSD activation, similar to the relative rearrangement of S4 and S0 (Pantazis et al., 2010b). On the other hand, membrane depolarization causes S2 to approach S1, whereas the principal voltage-sensing helices of BK, S2 and S4, are within collisional distance at rest and diverge upon activation.

MATERIALS AND METHODS

Molecular biology

For site-directed fluorescence labeling with a thiol-reactive fluorophore, an hSlo clone (provided by L. Toro, University of California, Los Angeles, Los Angeles, CA; NCBI Protein database accession no. U11058) (Wallner et al., 1995) transcribed from the fourth methionine without extracellular cysteines (C14S, C141S, and C277S), was used. Background mutation R207Q was introduced to increase P_O at low $[Ca^{2+}]_i$ (Díaz et al., 1998; Ma et al., 2006) and to be consistent with the previous fluorometric investigations of the human BK channel voltage sensor (Savalli et al., 2006, 2007, 2012; Pantazis et al., 2010a,b). A single cysteine was substituted at positions at the extracellular flank of S1 (S135C) or S2 (Y145C) for subsequent modification by thiol-reactive fluorescent labels, and Trp residues were substituted at positions along the S1–S2 extracellular linker. Single-point mutations were generated with QuikChange Site-Directed Mutagenesis kit (Agilent Technologies) and confirmed by sequencing. The cDNAs were transcribed to cRNAs in vitro (mMESSAGE MACHINE; Ambion) and stored at −80°C.

Oocyte preparation

Xenopus laevis (Nasco) oocytes (stage V–VI) were prepared as described previously (Haug et al., 2004) and then injected with 50 nl of total cRNA (0.1–0.5 μg/μl) using a nanoinjector (Drummond Scientific). Injected oocytes were maintained at 18°C in an amphibian saline solution supplemented with 50 μg/ml gentamycin (Gibco), 200 μM DTT, and 10 μM EDTA. 3–6 d after injection, oocytes were stained for 40 min with 10 μM of membrane-impermeable, thiol-reactive fluorophore, tetramethylrhodamine-5′-maleimide (TMRM; AnaSpec), in a depolarizing solution (in mM: 120 K-methanesulfonate [MES], 2 $Ca(MES)_2$, and 10 HEPES, pH 7.0) at 18°C in the dark. Alternatively, oocytes were incubated with 20 μM MTS-TAMRA (Santa Cruz Biotechnology, Inc.) for 40 s on ice. 100 mM of fluorescent probe stock was dissolved in DMSO and stored at −20°C. After fluorescent labeling, the oocytes were rinsed in dye-free saline before being mounted in the recording chamber. Both TMRM and MTS-TAMRA are rhodamine-based fluorescent labels that can be collisionally quenched by photo-induced e^- transfer by Trp residues (Doose et al., 2005, 2009; Mansoor et al., 2010; Pantazis et al., 2010b).

Electrophysiological techniques

The cut-open oocyte voltage clamp. The cut-open oocyte Vaseline gap technique is a low-noise, fast-clamp technique (Stefani and Bezanilla, 1998). The oocyte is placed in a triple-compartment Perspex chamber, with a diameter of 600 μm for the top and bottom apertures. The top chamber isolates the oocyte's upper domus and maintains it under clamp. The middle chamber provides a guard shield by clamping the middle part of the oocyte to the same potential as the top chamber. The bottom chamber injects current intracellularly through the saponin-permeabilized part of the oocyte. Fluorescence emission and ionic current were simultaneously measured from the same area of membrane isolated by the top chamber (Cha and Bezanilla, 1997; Gandhi and Olcese, 2008). The optical setup consists of a microscope (Axioscope FS; Carl Zeiss) with filters (Semrock) appropriate for rhodamine excitation and emission wavelengths. The light source is a 100-W

microscope halogen lamp. A TTL-triggered shutter (Uniblitz VS 25; Vincent Associates) is mounted on the excitation light path. The objective (40×, water immersion; LUMPlanFl; Olympus) has a numerical aperture of 0.8 and a working distance of 3.3 mm (Olympus), which leaves enough room for the insertion of the microelectrode. The emission light is focused on a photodiode (PIN-08-GL; UDT Technologies). An amplifier (Photomax 200; Dagan) is used for the amplification of the photocurrent and background fluorescence subtraction. The external solution contained (mM): 110 Na-MES, 10 K-MES, 2 $Ca(MES)_2$, and 10 Na-HEPES, pH 7.0. The internal solution contained (mM): 120 K-glutamate and 10 HEPES, pH 7.0. Standard solution for the intracellular recording micropipette is (in mM): 2,700 Na-MES and 10 NaCl. Low access resistance to the oocyte interior was obtained by permeabilizing the oocyte with 0.1% saponin carried by the internal solution.

Analysis. Experimental data were recorded and analyzed with a customized program developed in our division. The G-V curves were calculated by dividing the I-V relationships (I-V curves) by the driving force ($V_m - E_K$), where V_m is the membrane potential and E_K is the equilibrium potential for K^+, estimated using the Nernst equation. Data for the membrane conductance (G-V) and the fluorescence (ΔF(V)) curves were fitted to one or two Boltzmann distributions of the form:

$$G(V) = \frac{G_{max}}{1 + e^{\left[z(V0.5 - Vm)\left(\frac{F}{RT}\right)\right]}}$$

$$\Delta F(V) = \frac{\Delta F_{max} - \Delta F_{min}}{1 + e^{\left[z(V0.5 - Vm)\left(\frac{F}{RT}\right)\right]}} - \Delta F_{min},$$

where G_{max} and ΔF_{max} are the maximal G and ΔF; ΔF_{min} is the minimal ΔF; z is the effective valence of the distribution; $V_{0.5}$ is the half-activating potential; V_m is the membrane potential; and F, R, and T are the usual thermodynamic values. Fitting was performed by least squares in Microsoft Excel. To characterize the overall voltage-dependent ΔF reported from a label, we normalized the total fluorescence change ($\Delta F_{total} = \Delta F_{max} - \Delta F_{min}$) and normalized by background fluorescence (F_0) and maximal conductance (G_{max}):

$$\frac{\Delta F_{total}}{F_0 \cdot G_{max}}.$$

Online supplemental material

In Fig. S1, the Trp side chain can quench a thiol-reactive fluorophore, PyMPO maleimide, in solution. In a previous investigation (Savalli et al., 2006), PyMPO labeling position 202, outside S4, reported slow voltage-dependent ΔF in the presence of W203. As PyMPO can be quenched by the Trp side chain, the reported ΔF can be interpreted as the rearrangement of S4, with respect to the S3–S4 linker, over a slow (200-ms) time course. Fig. S1 is available at http://www.jgp.org/cgi/content/full/jgp.201210807/DC1.

RESULTS

Voltage-dependent ΔF signals reported from the extracellular flank of the S1 helix track voltage sensor activation and require W203 at the extracellular flank of S4

S1 is a hydrophobic helix, possessing no charges that contribute to the BK channel voltage-sensing process (Ma et al., 2006). However, considering the close packing of the VSD helix bundle in the membrane (Long et al., 2007), the BK S1 is likely intimately associated with segments S2, S3, and S4 (Fig. 1 D), which do carry voltage-sensing charges (Ma et al., 2006) and undergo

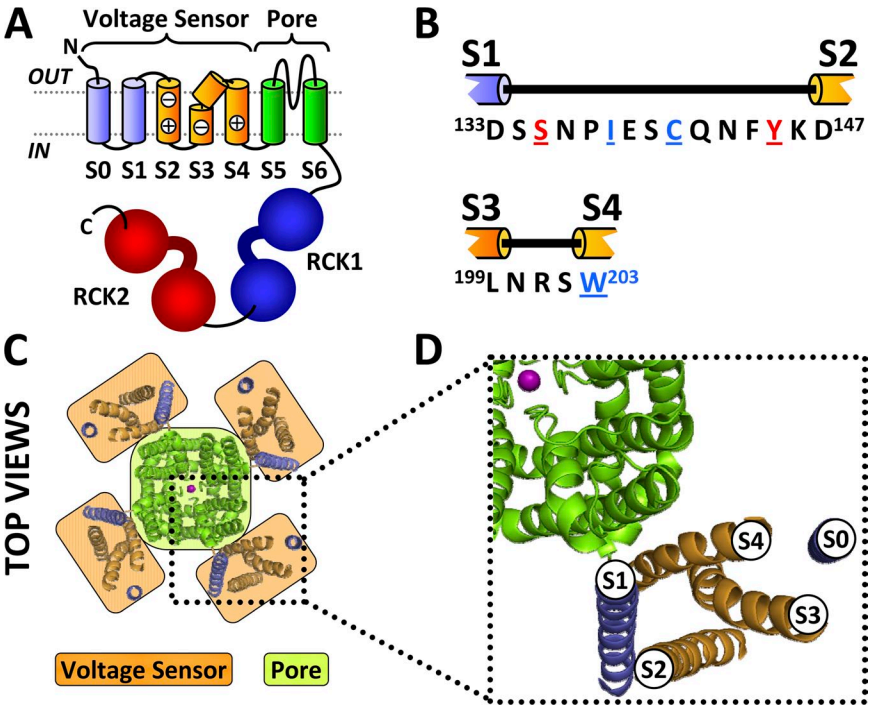

Figure 1. BK channel topology and assembly. (A) Membrane topology of a BK α subunit (Wallner et al., 1996; Meera et al., 1997). Voltage-sensing charged residues D153 and R167 (S2), D186 (S3), and R213 (S4) (Ma et al., 2006) are indicated by their charge polarity. (B) The sequences of the human BK extracellular S1–S2 (S134–K146) and S3–S4 (N200–S202) linkers, which include positions pertinent to this work: cysteine substitutions for fluorescent labeling (in red: S135C and Y145C) and Trp introductions for fluorophore quenching (in blue: I138W and C141W; note that C141 is normally substituted to serine to prevent fluorophore conjugation). The native Trp at the extracellular tip of S4 (W203) is also in blue. (C) Top view of a potassium channel transmembrane domain (K_V1.2–2.1 chimera; Protein Data Bank accession no. 2R9R; Long et al., 2007) with the addition of S0 ideal α helices to resemble BK channels. The pore domain (green) contains a K^+ ion and is surrounded by four VSD helix bundles (orange). (D) Suggested packing arrangement of the BK VSD helix bundle (Liu et al., 2010).

voltage-dependent conformational changes (Savalli et al., 2006; Pantazis et al., 2010a). To probe for voltage-dependent conformational rearrangements in the vicinity of the extracellular flank of S1, we substituted a unique cysteine at position 135 (S135C) and labeled the channel with MTS-TAMRA (Fig. 2 A). Positive depolarization-evoked ΔF was observed with a voltage dependence that preceded that of ionic conductance (Fig. 2 B), indicating that the ΔF reported structural rearrangements of the voltage sensor. The voltage dependence of S1-reported ΔF was very similar to that of the ΔF of TMRM labeling the extracellular flank of S4 (Savalli et al., 2006, 2007, 2012; Pantazis et al., 2010a) and S0 (Pantazis et al., 2010b). The ΔF reported by the S0 label was found to be caused by its state-dependent quenching by a Trp residue at the extracellular tip of S4, W203 (Pantazis et al., 2010b).

To test whether W203 is also responsible for the quenching of S1-conjugated fluorophores, we removed it by mutation W203V (Fig. 2 C), as previously (Savalli et al., 2006, 2007, 2012; Pantazis et al., 2010a,b). MTS-TAMRA ΔF reported from position 135 in W203V channels was strongly attenuated (Fig. 2, D and E). The voltage dependence of this residual ΔF signal was similar to that from channels without the W203V mutation (Fig. 2 F), indicating that the observed decrease in ΔF amplitude was caused by attenuation of the fluorophore quenching process that gave rise to the observed fluorescence deflections, rather than a shift in voltage dependence.

W203, at the extracellular end of S4, is the principal quencher of fluorescence reported from S2

To investigate how S2 and S4 rearrange with respect to each other, we labeled S2 (position 145) with TMRM (Fig. 3 A), resolving positive fluorescence deflections (Fig. 3 B) indicating protein rearrangements with a voltage dependence similar to those reported by S4-, S0-, and S1-labeled channels. Substitution of W203, extracellular to S4 (W203V) (Fig. 3 C), resulted in an attenuation of the reported ΔF (Fig. 3, D and E). The ΔF reported from S2 recapitulates those reported from S0 (Pantazis et al., 2010b) and S1 (Fig. 2), suggesting that the side chain of W203, at S4, interacts with fluorophore-labeling segments S0, S1, and S2 in a voltage-dependent manner. The voltage dependence of the residual ΔF reported from S2 in W203V channels was right-shifted toward more depolarized potentials (Fig. 3, D and F). In a previous work, we reported that ΔF from TMRM-labeling S2 in W203V channels differs significantly in terms of voltage dependence and kinetics from the ΔF

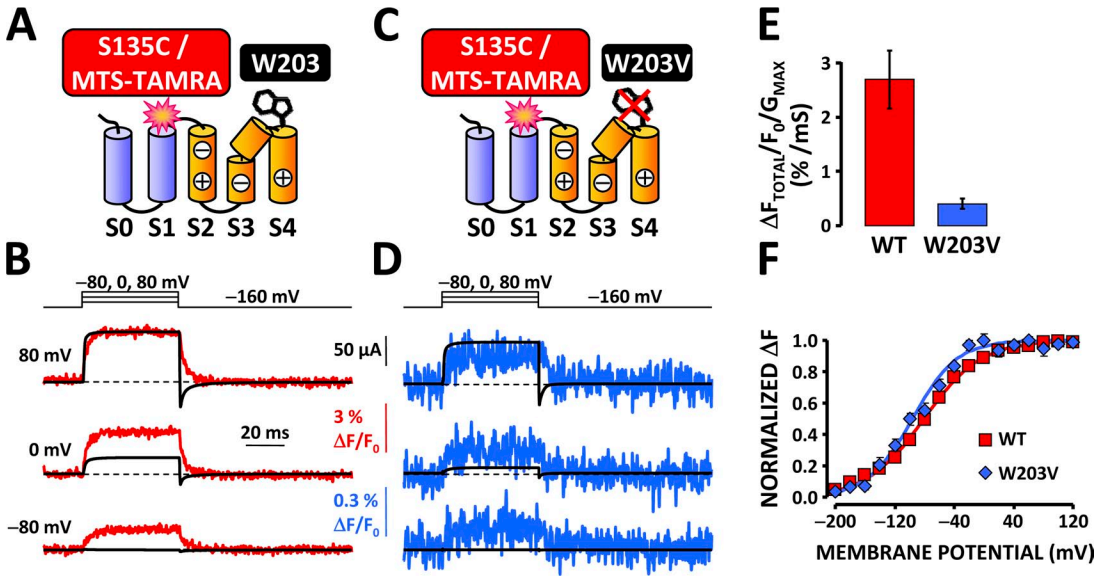

Figure 2. Voltage-dependent ΔF reported from the S1 extracellular flank is abolished by substitution of W203 at the extracellular flank of S4. (A) Illustration of the BK channel construct used; only the VSD transmembrane helices of one subunit are shown. A unique cysteine was substituted at the extracellular flank of S1 (S135C) and covalently labeled with fluorophore MTS-TAMRA to resolve conformational rearrangements from this region. (B) Voltage-pulse protocol, characteristic evoked K^+ currents (black), and simultaneously recorded MTS-TAMRA fluorescence (red) from the BK channel construct illustrated above. ΔF voltage dependence: $V_{0.5} = -81 \pm 4$ mV and $z = 0.68 \pm 0.04$ e^0. Conductance–voltage dependence: $V_{0.5} = -29 \pm 7$ mV and $z = 0.86 \pm 0.03$ e^0; $n = 11$. (C and D) As in A and B, for channels with the additional mutation W203V to remove the native Trp at the extracellular portion of S4. MTS-TAMRA fluorescence traces are in blue. Note that the fluorescence scale is 10 times that for wild-type (WT) channels. ΔF voltage dependence: $V_{0.5} = -97 \pm 2$ mV and $z = 0.84 \pm 0.04$ e^0. Conductance–voltage dependence: $V_{0.5} = 32 \pm 2$ mV and $z = 0.99 \pm 0.06$ e^0; $n = 5$. (E) Mean fitted $\Delta F_{total}/F_0$ signal, normalized for fitted maximal conductance for WT (red; $\Delta F_{total}/F_0/G_{max} = 1.8 \pm 0.42\%/mS$) and W203V (blue; $\Delta F_{total}/F_0/G_{max} = 0.41 \pm 0.09\%/mS$) channels. Mutation W203V attenuated the ΔF reported by MTS-TAMRA from position 135 by ≈85%. (F) Mean, normalized ΔF from WT (red squares) or W203V (blue diamonds) BK channels labeled at position 135 with MTS-TAMRA. Error bars represent SEM.

reported from S4, in BK channels with intact voltage sensing as well as those with voltage-sensing charge neutralizations, postulating that they reflect the intrinsic voltage dependence of helix S2 (Pantazis et al., 2010a).

In the next experiments, we provide evidence that, even though the fluorescence deflections reported from the extracellular flanks of S1 and S2 are similar in voltage dependence and dependence on W203, the two segments do no behave as a single structural unit, but they undergo a relative rearrangement upon membrane depolarization.

Resolving the relative voltage-dependent rearrangement of S1 and S2 by manipulating the quenching environment of the fluorescent label with site-directed Trp substitution

The S2 helix of the BK VSD bears two charged residues that contribute to the voltage-sensing charge: D153 and R167 (Ma et al., 2006). As such, S2 would be expected to rearrange with respect to the electric field upon depolarization. Accordingly, TMRM labels attached to S2 (in W203V channels, as in Fig. 3 D) exhibit ΔF with distinct kinetics and voltage dependence to the ΔF of S4 labels, strongly suggesting that S2 undergoes conformational changes upon depolarization (Pantazis et al., 2010a). On the other hand, S1 bears no voltage-sensing charges and is therefore unlikely to undergo large conformational changes upon membrane depolarization. Because of the physical proximity of the two helices and difference in their expected behavior upon depolarization, we reasoned that the two segments also undergo a voltage-dependent relative rearrangement, and sought to resolve it by directly manipulating the environment of the S1-conjugated fluorescent label by the introduction of a Trp residue extracellular to S2.

Fig. 4 summarizes the results of substituting Trp in two positions along the S1–S2 linker, in channels fluorescently labeled with MTS-TAMRA at the extracellular portion of S1 (position 135). Fig. 4 (A–D) demonstrates a condition similar to that shown in Fig. 2 (A and B), whereby the label reports positive ΔF upon depolarization, which was subsequently shown to be caused by voltage-dependent interaction of the S1 fluorophore with the side chain of the S4 tryptophan, W203 (Fig. 2). When a Trp is substituted near S2 in the S1–S2 linker (Fig. 4 E, C141W), MTS-TAMRA–labeling position 135 (outside S1) reports a complex fluorescence signal upon depolarization (Fig. 4 G). In addition to the dequenching component, which is caused by the rearrangement of S1 and S4 (Figs. 2 and 4 C), a voltage-dependent quenching component is evident, which demonstrates the state-dependent

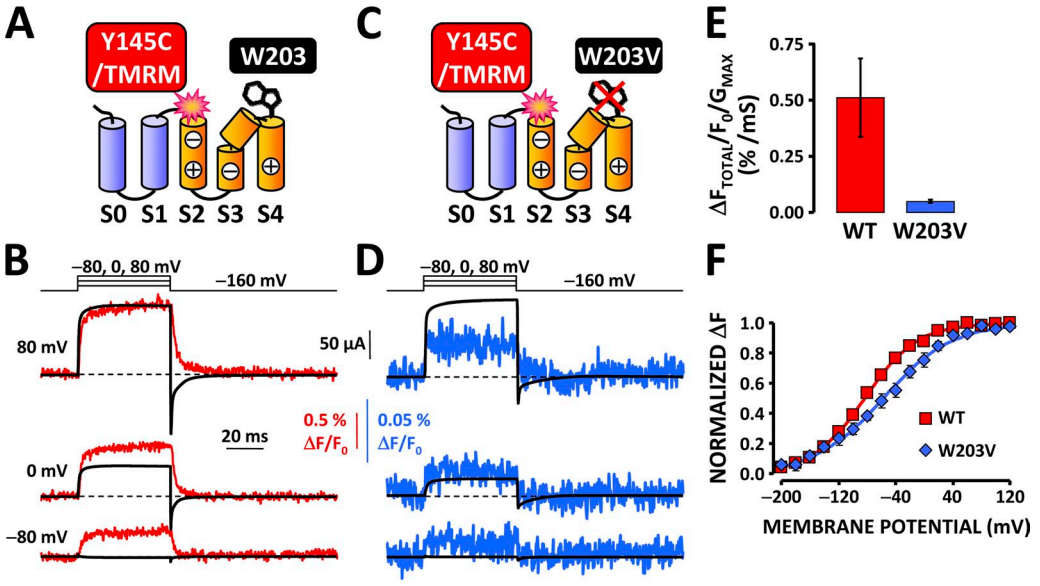

Figure 3. W203, outside S4, is the principal quencher of ΔF reported from S2. (A) Illustration of the BK channel construct used; only the VSD transmembrane helices of one subunit are shown. A unique cysteine was substituted at the extracellular flank of S2 (Y145C) and covalently labeled with fluorophore TMRM to resolve conformational rearrangements from this region. (B) Voltage-pulse protocol, characteristic evoked K^+ currents (black), and simultaneously recorded TMRM fluorescence (red) from the BK channel construct illustrated above. ΔF voltage dependence: $V_{0.5} = -82 \pm 5$ mV and $z = 0.74 \pm 0.05$ e^0. Conductance–voltage dependence: $V_{0.5} = -26 \pm 10$ mV and $z = 1.2 \pm 0.11$ e^0; $n = 14$. (C and D) As in A and B, for channels with the additional mutation W203V to remove the Trp residue at the extracellular portion of S4. TMRM fluorescence traces are in blue. Note that the fluorescence scale is 10 times that for WT channels. ΔF voltage dependence: $V_{0.5} = -58 \pm 9$ mV and $z = 0.57 \pm 0.05$ e^0. Conductance–voltage dependence: $V_{0.5} = 10 \pm 2$ mV and $z = 0.86 \pm 0.1$ e^0; $n = 8$. (E) Mean fitted $\Delta F_{total}/F_0$ signal, normalized for fitted maximum conductance to normalize for channel expression for WT (red; $\Delta F_{total}/F_0/G_{max} = 0.51 \pm 0.17\%/mS$) and W203V (blue; $\Delta F_{total}/F_0/G_{max} = 0.05 \pm 0.007\%/mS$) channels. Mutation W203V attenuated the ΔF reported by TMRM from position 145 by ≈90%. (F) Mean, normalized ΔF from WT (red squares) or W203V (blue diamonds) BK channels labeled at position 145 with TMRM. Error bars represent SEM.

interaction of the S1 label with W141, near S2. The unquenching component responsible for the fluorescence transients was absent in channels lacking the native S4 tryptophan (Fig. 4, I and K, W203V). However, the concurrent removal of native W203 and the introduction of W141 resulted in a highly shifted voltage dependence of activation (Fig. 4 J).

To further probe the photochemistry of Trp introduction in the S1–S2 linker, we introduced a Trp closer to the fluorescent label (Fig. 4 M, I138W). This resulted in the almost complete absence of fluorescence deflections (Fig. 4 O), likely caused by static, voltage-independent quenching of fluorophore by W138 (Doose et al., 2005; Mansoor et al., 2010). A weak fluorescence transient is consistently observed upon sufficient depolarizations (Fig. 4 P). Although the molecular events underlying these fluorescence dynamics are unclear, their presence confirms that MTS-TAMRA did modify C135, and the lack of ΔF reported from I138W channels is caused by the static photochemical interaction of W138 and the C135-conjugated label.

DISCUSSION

Model-independent inference of dynamic structural information from voltage-clamp fluorometry data

The BK channel VSD is an ideal system to try and test the principles of structurally assigned voltage-clamp fluorometry by optically tracking the photochemical

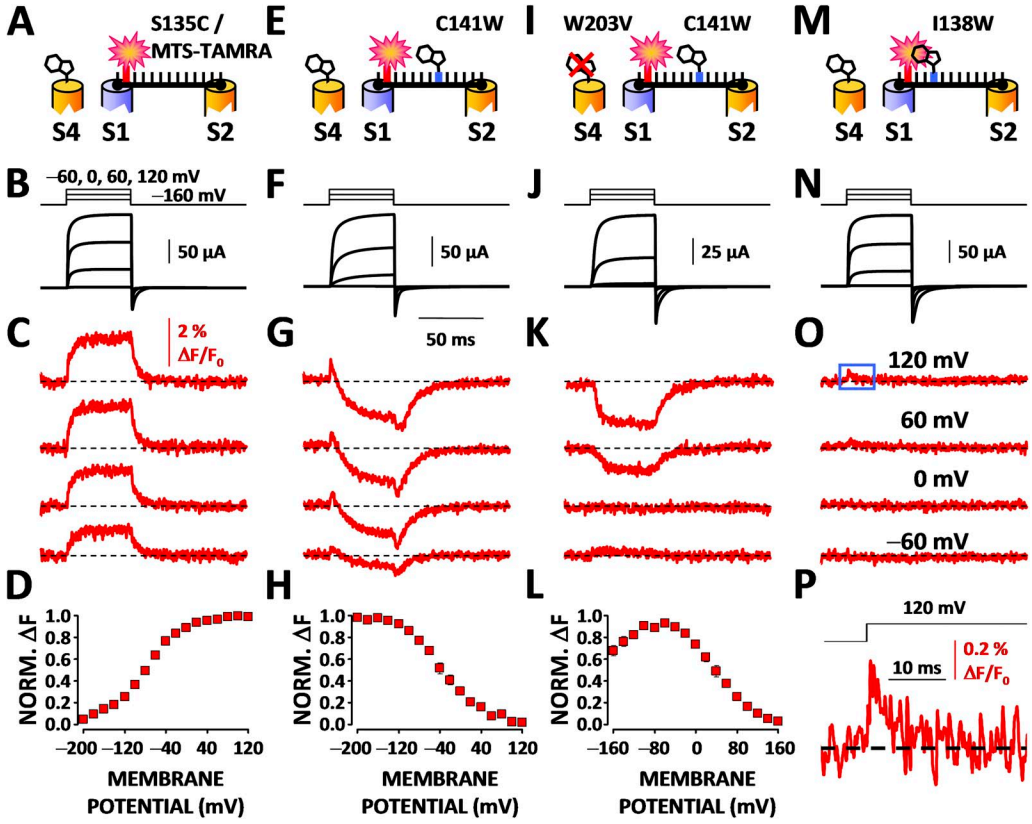

Figure 4. Quenching the S1-conjugated fluorescent label with introduced tryptophans in the S1–S2 linker. (A) Illustration of the BK channel construct used; only the extracellular flanks of S1, S2, and S4 are shown. The intervals in the S1–S2 linker (S134–K146; Fig. 1 B) represent its residues. As in Fig. 2 A, a unique cysteine was substituted at the extracellular flank of S1 (S135C) and covalently labeled with fluorophore MTS-TAMRA. (B) Voltage-pulse protocol and characteristic evoked K^+ currents (black) from the BK channel construct illustrated above, as in Fig. 2 B. (C) MTS-TAMRA fluorescence traces simultaneously recorded with the current traces above, which were shown in Fig. 2 to be dependent on W203 (at S4). (D) Mean, normalized ΔF, as in Fig. 2 F. (E–H) As in A–D, for S135C, MTS-TAMRA–labeled channels with the additional mutation C141W to introduce a Trp at the S1–S2 linker, near S2. Note the additional voltage-dependent quenching component. Conductance–voltage dependence: $V_{0.5} = -6 \pm 5$ mV and $z = 0.79 \pm 0.04$ e^0; $n = 6$. Note that in all other constructs, C141 has been substituted by serine to prevent fluorophore labeling. (I–L) As in E–H, with the additional mutation W203V to remove the native Trp at the extracellular flank of S4. Note that the fluorescence transients observed in G are abolished. Conductance–voltage dependence: $V_{0.5} = 61 \pm 6$ mV and $z = 0.99 \pm 0.04$ e^0; $n = 13$. The small unquenching component observed at hyperpolarized potentials is probably the same as that observed in the S135C–W203V channel (Fig. 2 D). (M–O) As in A–C, for S135C, MTS-TAMRA–labeled channels with the additional mutation I138W to introduce a Trp residue near the fluorophore position. The apparent lack of ΔF could indicate lack of MTS-TAMRA conjugation or static (voltage-independent) quenching of the fluorophore by the nearby W138. (P) An expansion of the time and fluorescence scales for the 120-mV depolarization in O to better demonstrate the transient, but consistently observed, unquenching of the fluorescence upon sufficient depolarization, confirming the fluorescent labeling of C135.

interaction between a fluorophore and Trp attached to specific positions in the protein: first, the property of the W203 side chain, at S4, to collide with and quench small fluorophores attached to positions around it according to the state of the VSD, revealing the relative movement of S4 with respect to nearby fluorescently labeled helices (Fig. 6) (Pantazis et al., 2010b); second, the S1–S2 system, which consists of the charge-bearing S2 (Ma et al., 2006), which rearranges with respect to the electric field upon depolarization (Pantazis et al., 2010a), and voltage-insensitive S1 (Ma et al., 2006), connected with S2 via a short extracellular linker. This provided the ideal platform to detect the relative voltage-dependent rearrangement that would be expected to occur between a voltage-sensitive and a voltage-insensitive transmembrane helix, by combining site-specific fluorescent labeling at an extracellularly accessible position near S1, and Trp introduction near S2, to induce Trp-mediated quenching (Figs. 4, A–L, and 5, B and C). We have combined the structural information from this work with the findings of previous investigations on BK channels and the $K_V1.2$–2.1 atomic structure (Long et al., 2007) to propose the rearrangements of the human BK channel VSD shown in Fig. 6, without applying a computational model. Nevertheless, because the fluorescence deflections reported by Trp-induced quenching reflect the probability of Trp–fluorophore collisions, the fluorescence data can be used as important constraints for, and to reduce the a priori assumptions of, the elaborate computational modeling of molecular rearrangements involved in voltage-dependent activation.

A potential limitation of manipulating the quenching of small protein-labeling fluorophores with targeted Trp introduction (or the removal of native Trp residues) is the risk of perturbing channel operation and gating. We have previously reported that substitution of the native W203 in BK channels results in a depolarizing shift of channel activation (Savalli et al., 2006; Pantazis et al., 2010b), which is also observed in this work (Figs. 2 and 3). The addition of Trp residues in the S1–S2 linker resulted in a less pronounced effect on channel activation (Fig. 4, F and N), which appeared to be cumulative to W203 substitution (Fig. 4 J). However, the characteristics

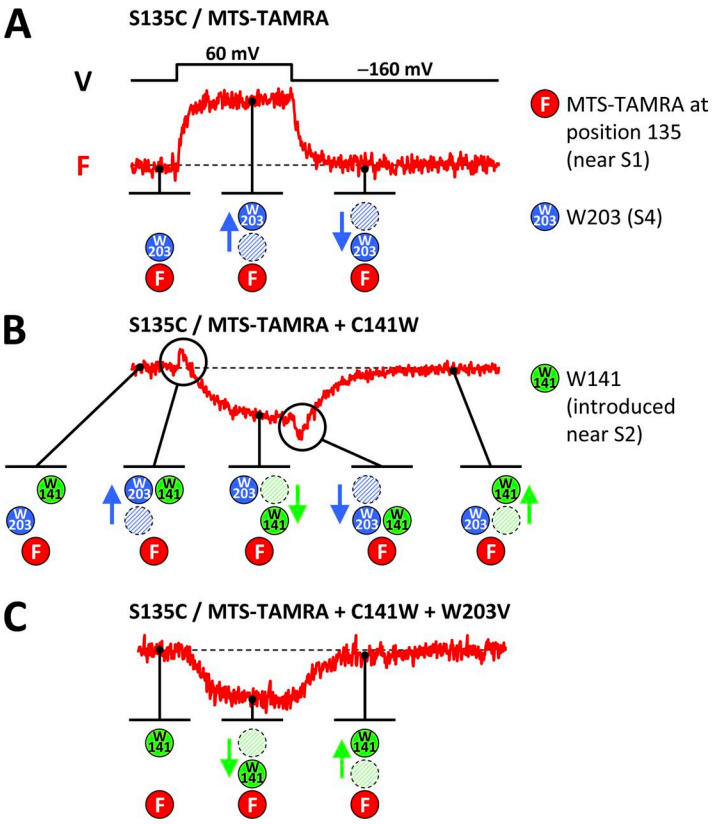

Figure 5. A photochemical interpretation of the observed fluorescence deflections. (A) A representative fluorescence trace recorded upon a 50-ms depolarization to 60 mV from channels labeled with MTS-TAMRA at position 135, at the S1 extracellular flank, in the presence of the native W203 (S4), as in Figs. 2 and 4 (A–D). At rest, the fluorophore is efficiently quenched by the Trp at S4 (W203), so that the reported fluorescence is relatively dim. Upon depolarization, the quenching efficiency of W203 decreases, so that overall fluorescence emission is increased and a positive ΔF is observed. The same interpretation was previously applied for TMRM fluorophore labeling the extracellular portion of S0 (Pantazis et al., 2010b) and can also account for the ΔF signals from TMRM-labeling S2, as their amplitude is also strongly attenuated by mutation W203V (Fig. 3). (B) A representative fluorescence trace recorded upon a 50-ms depolarization to 60 mV from channels labeled with MTS-TAMRA at position 135, at the S1 extracellular flank, in the presence of the native W203 (S4) and introduced W141 (near S2; Fig. 4, E–H). At rest, W203 quenches the fluorophore (as in A), whereas W141 quenches the fluorophore relatively less, so that the overall fluorescence detected is at an intermediate level. Upon depolarization, W203 quenching is lifted, generating positive ΔF, as in A. At the same time, W141 approaches and quenches the fluorophore. It seems that the W141 is a more efficient quencher than W203, as the overall fluorescence level at the depolarized state is dimmer than when at rest. However, W203 departure appears to have faster kinetics than W141 quenching, so it is observed as an upward transient deflection. Upon membrane repolarization, the two quenching processes are reversed: W203 returns to quench the label, so that overall fluorescence becomes transiently dimmer, whereas W141 departs, reducing its quenching efficiency. (C) A representative fluorescence trace recorded upon a 50-ms depolarization to 60 mV from channels labeled with MTS-TAMRA at position 135, at the S1 extracellular flank, in the presence of the introduced W141 (near S2), with additional mutation W203V to remove the native W203 (S4; as in Fig. 4, I–L). The fluorescent label is apparently unquenched at rest, as W203 has been substituted. Upon depolarization, W141 approaches and quenches the fluorophore, a process reported as a negative ΔF. Upon membrane repolarization, W141 departs, reducing its quenching efficiency. In agreement with the ΔF interpretation in A and B, the substitution of W203 resulted in the lack of observable depolarization-induced positive ΔF.

of the observed fluorescence deflections of the clones studied in this work cannot be readily accounted for by changes of the voltage dependence of channel activation, whereas the photochemical interpretation of the data (Fig. 5) is consistent with the fluorescence characteristics of all the clones studied in this and previous (Pantazis et al., 2010b) work.

Converging toward a dynamic map of voltage-dependent structural rearrangements in the BK voltage sensor

The fluorescence data from S1-conjugated MTS-TAMRA in channels with or without the native Trp outside S4 (Fig. 2, W203) recapitulate the fluorescence of S0-labeling TMRM, in that the positive depolarization-induced ΔF is strongly attenuated by removal of the S4 Trp (W203V) (Pantazis et al., 2010b). As such, the same structural interpretation can account for these data: the extracellular portions of S1 and S4 appear to be within collisional range at rest, so that the S1 label is efficiently quenched by the W203 side chain in S4; however, upon depolarization, the distance between the two helices increases, reducing the efficiency of W203-induced quenching, so that a positive fluorescence deflection is observed (Fig. 5 A). According to Liu et al. (2010), S1 and S0 are almost diametrically opposite S4 on the plane of the membrane (Fig. 1 D). S4 could move away from S1 and S0, as the positively charged, voltage-sensing R213 (Ma et al., 2006) moves outward with respect to the electric field. Such a motion was previously suggested to explain the fluorescence from S0 labels (Pantazis et al., 2010b) and can be used to account for the fluorescence deflections reported from S1 as well (Fig. 6).

Introduction of a Trp near the extracellular flank of S2 (C141W) imposed a depolarization-dependent quenching component (negative ΔF; Fig. 4, G and K) to the fluorescence of MTS-TAMRA label conjugated to S1 (position 135), revealing that the fluorophore and W141 converge upon activation (Fig. 5, B and C). S2 bears two residues that contribute to the voltage-sensing charge of BK: negatively charged D153 at the extracellular half of the helix and positively charged R167 at the intracellular end (Ma et al., 2006), exhibiting intrinsic voltage-sensing properties (Pantazis et al., 2010a). Upon membrane depolarization, D153 would be compelled to move inward and R167 outward, inducing S2 to tilt. Because S1 does not possess sensing charges (Ma et al., 2006), it is likely that S2 tilting toward S1 gives rise to the relative rearrangement of the two segments. Such a movement is included in the proposed structural interpretation of the results in Fig. 6.

A large component of the ΔF signal from labels on S2 arises from its state-dependent interaction with W203 in S4 (Fig. 3), so that the molecular quenching interpretation in Fig. 5 A can also account for the ΔF reported from S2 labels. The data suggest that S2 and S4 are within collisional range at rest but follow different paths upon activation, so that their extracellular flanks diverge. This interpretation is also consistent with the findings that S2 approaches S1 upon activation, but S4 and S1 diverge, and has been considered in constructing the proposed voltage-dependent rearrangements of the BK channel VSD shown in Fig. 6.

How does S3 rearrange with respect to other helices?

We did not directly probe for the motions of S3 relative to the other VSD helices in this work. The extracellular linker between S3 and S4 in the BK VSD is very short, consisting of three residues (N200–R201–S202; Fig. 1 B) and exhibiting secondary structure (Semenova et al., 2009;

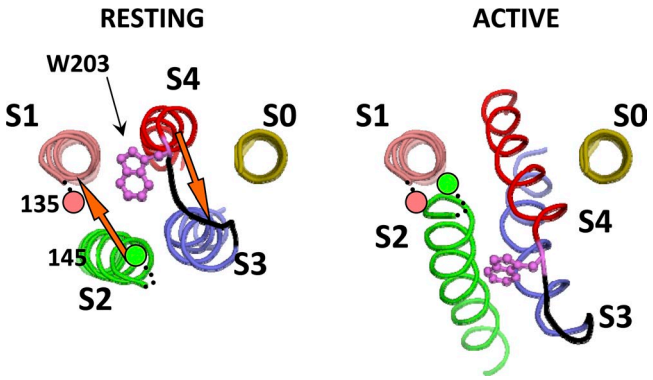

Figure 6. A possible model-independent structural interpretation of the fluorescence data. (Left) A hypothetical model of the BK VSD helices at rest. It is based on our previous illustration of BK VSD helices S0, S3, and S4 (Pantazis et al., 2010b), with the addition of S1 and S2. Helices S1–S4 are arranged in a counterclockwise bundle with the structure of their homologous helices in the $K_V1.2$–2.1 crystal structure (Protein Data Bank accession no. 2R9R; Long et al., 2007). S0, modeled as an ideal α helix, is positioned according to the most recent information from disulfide cross-linking efficiency (Liu et al., 2010). S3 and S4 are connected by a short extracellular helix–loop–helix structure as inferred previously by bimane fluorescence scanning (Semenova et al., 2009). The native S4 Trp, W203, is shown in violet, and hypothetical positions for fluorophore conjugation cysteines in S1 (135) and S2 (145) are also indicated. The extracellular flank of S4 is relatively close to those of S0, S1, and S2, so that fluorophores labeling S0 (Pantazis et al., 2010b), S1 (Fig. 2), and S2 (Fig. 3) are efficiently quenched by W203 (Fig. 5 A). (Right) Membrane depolarization induces voltage-sensing residue R213 (S4) to move outward and D186 (S3) inward (Ma et al., 2006), causing the rearrangement of S3 and S4 with respect to the electric field (Savalli et al., 2006; Pantazis et al., 2010a). This results in a relative rearrangement between the voltage-sensing S3/S4 and S0 and S1, lifting the quenching effect of W203 to fluorophores labeling S0 (Pantazis et al., 2010b) or S1 (Figs. 2 and 5 A). S2 is shown to undergo a tilting motion upon depolarization, hypothetically induced by its voltage-sensing residues D153 and R167 (Ma et al., 2006; Pantazis et al., 2010a), causing its extracellular flank to diverge from W203 (S4) and move toward S1, consistent with the fluorescence data in this work, whereby an S2-conjugated fluorophore (position 145) is quenched by W203 (S4; violet) at rest (Figs. 3 and 5 A), whereas an S1-conjugated fluorophore (position 135) is quenched by an introduced Trp near S2 upon activation (Figs. 4, E–L, and 5, B and C). The image was made with PyMOL 0.99 (DeLano Scientific).

Unnerståle et al., 2009). Because S4 and the extracellular portion of S3 (S3b) are connected by a very short and structurally robust tether in BK, we propose that the collisional events between the S4 Trp (W203) and S0-, S1-, and S2-labeling fluorophores represent, to the best of our current knowledge, the rearrangements of an S4–S3b unit. When PyMPO maleimide is used to label position 202, a positive voltage-dependent ΔF is reported that is abolished by W203V (Savalli et al., 2006). Because the Trp side chain can also quench PyMPO fluorescence (Stern–Volmer bimolecular quenching constant: 129 M^{-1}; Fig. S1), this result is consistent with a conformational change between these two positions. This rearrangement occurs over a longer time course (≈200 ms) than those reported in this work and may represent reorganizations of the BK VSD occurring while the channel gate is open (Savalli et al., 2006).

How do mechanical interactions contribute to the BK voltage-sensing process?

In a previous work on the functional interaction of S2 and S4 in the BK VSD (Pantazis et al., 2010a), we proposed two mechanisms of cooperativity between the two voltage-sensing helices: in the first, S2 and S4 are mechanically coupled, so that the voltage-sensing charge of one helix contributes to that of the other; the second mechanism involves mutual state-dependent focusing of the electric field by dynamic aqueous crevice formation, inspired by previous hypotheses in the literature (Cha and Bezanilla, 1997; Chanda and Bezanilla, 2008). Although the two scenarios are not mutually exclusive, the work presented here contributes more weight to the idea of dynamic focusing of the electric field, which is more consistent with S2 and S4 undergoing different and divergent motions, whereas mechanical interactions might be expected to result in movements of uniform direction.

On the other hand, the Trp-induced quenching mechanism used to resolve the relative helical rearrangements, including those of S2 and S4, relies on electron waveform overlap, i.e., a collision event (Doose et al., 2005, 2009; Mansoor et al., 2010). Because the S4 Trp (W203) quenches S0-, S1-, and S2-labeling fluorophores more efficiently as the membrane potential repolarizes, it would appear that S4 "nudges" S0, S1, and S2 upon VSD deactivation, whereas S2 collides with S1 more frequently in the active state.

The collisions, or mechanical interactions, between VSD segments resolved previously (Pantazis et al., 2010b) and in this work (Fig. 6) could be an important aspect of voltage sensing, which, after all, is an electromechanical process. The mechanical interaction of voltage-sensing helices S2 and S4 may enhance their voltage-sensing properties (Pantazis et al., 2010a). Furthermore, the interactions of voltage-sensing S2 and S4 with voltage-insensitive S0 and S1 could also contribute to the efficiency with which the VSD actuates voltage-dependent channel gating: S0 and S1 likely pose steric constraints or even mechanical guidance and support to the movements of the voltage-sensing S2 and S4. Thus, the interaction of auxiliary β subunits with S0 and S1 (Wallner et al., 1996; Meera et al., 1997; Morrow et al., 2006; Wu et al., 2009; Liu et al., 2010; Morera et al., 2012) may contribute to the modulating effect of β subunits to the BK voltage-sensing process (Orio et al., 2002; Bao and Cox, 2005; Orio and Latorre, 2005; Savalli et al., 2007; Lee et al., 2010; Wu and Marx, 2010; Sun et al., 2012). Moreover, the mutual coordination of Mg^{2+} between the intracellular ligand-sensing gating ring and D99, in the intracellular S0–S1 linker (Yang et al., 2008), could contribute to the functional coupling between the BK voltage- and ligand-sensing domains (Horrigan and Aldrich, 2002; Horrigan and Ma, 2008; Savalli et al., 2012). Finally, the palmitoylation site in the S0–S1 linker (Jeffries et al., 2010) suggests that the anchoring of helices S0 and S1 to the membrane could be important for their structural role in VSD operation.

By combining site-specific fluorescence labeling and quenching, we have resolved structural rearrangements occurring between assigned loci in the voltage sensor of human BK channels. We propose a possible structural interpretation of how this "non-canonical" VSD operates in Fig. 6. Specifically, we have resolved the direction of movement of the crucial voltage-sensing helices S4 and S2, and revealed their state-dependent mechanical interaction with S0, S1, and each other. Because the VSDs of a multitude of voltage-dependent proteins are structurally conserved (Nelson et al., 1999; Chanda and Bezanilla, 2008), we are confident that site-directed, Trp-induced collisional quenching of fluorescent labels can be used to resolve the relative motions of assigned positions in other VSD-activated proteins and provide crucial constraints for the elaborate computational modeling of voltage-dependent rearrangements.

We are grateful to members of the Olcese laboratory for critical comments on the manuscript. The *hSlo* clone was a kind gift from Ligia Toro (Dept. of Anesthesiology, UCLA).

This work was supported by research grants from National Institutes of Health/National Institute of General Medical Sciences (grant R01GM082289 to R. Olcese) and American Heart Association (Western States Affiliate) Postdoctoral Fellowship (grant 11POST7140046 to A. Pantazis).

Sharona E. Gordon served as editor.

Submitted: 26 March 2012
Accepted: 21 June 2012

REFERENCES

Armstrong, C.M. 2003. Voltage-gated K channels. *Sci. STKE.* 2003: re10. http://dx.doi.org/10.1126/stke.2003.188.re10

Bao, L., and D.H. Cox. 2005. Gating and ionic currents reveal how the BK_{Ca} channel's Ca^{2+} sensitivity is enhanced by its β1 subunit. *J. Gen. Physiol.* 126:393–412. http://dx.doi.org/10.1085/jgp.200509346

Bao, L., C. Kaldany, E.C. Holmstrand, and D.H. Cox. 2004. Mapping the BK_{Ca} channel's "Ca^{2+} bowl": side-chains essential for Ca^{2+} sensing. *J. Gen. Physiol.* 123:475–489. http://dx.doi.org/10.1085/jgp.200409052

Bezanilla, F. 2008. How membrane proteins sense voltage. *Nat. Rev. Mol. Cell Biol.* 9:323–332. http://dx.doi.org/10.1038/nrm2376

Bian, S., I. Favre, and E. Moczydlowski. 2001. Ca2+-binding activity of a COOH-terminal fragment of the Drosophila BK channel involved in Ca2+-dependent activation. *Proc. Natl. Acad. Sci. USA.* 98:4776–4781. http://dx.doi.org/10.1073/pnas.081072398

Cha, A., and F. Bezanilla. 1997. Characterizing voltage-dependent conformational changes in the Shaker K+ channel with fluorescence. *Neuron.* 19:1127–1140. http://dx.doi.org/10.1016/S0896-6273(00)80403-1

Chanda, B., and F. Bezanilla. 2008. A common pathway for charge transport through voltage-sensing domains. *Neuron.* 57:345–351. http://dx.doi.org/10.1016/j.neuron.2008.01.015

Claydon, T.W., and D. Fedida. 2007. Voltage clamp fluorimetry studies of mammalian voltage-gated K(+) channel gating. *Biochem. Soc. Trans.* 35:1080–1082. http://dx.doi.org/10.1042/BST0351080

Cui, J., and R.W. Aldrich. 2000. Allosteric linkage between voltage and Ca(2+)-dependent activation of BK-type mslo1 K(+) channels. *Biochemistry.* 39:15612–15619. http://dx.doi.org/10.1021/bi001509+

Cui, J., H. Yang, and U.S. Lee. 2009. Molecular mechanisms of BK channel activation. *Cell. Mol. Life Sci.* 66:852–875. http://dx.doi.org/10.1007/s00018-008-8609-x

Díaz, L., P. Meera, J. Amigo, E. Stefani, O. Alvarez, L. Toro, and R. Latorre. 1998. Role of the S4 segment in a voltage-dependent calcium-sensitive potassium (hSlo) channel. *J. Biol. Chem.* 273: 32430–32436. http://dx.doi.org/10.1074/jbc.273.49.32430

Doose, S., H. Neuweiler, and M. Sauer. 2005. A close look at fluorescence quenching of organic dyes by tryptophan. *ChemPhysChem.* 6:2277–2285. http://dx.doi.org/10.1002/cphc.200500191

Doose, S., H. Neuweiler, and M. Sauer. 2009. Fluorescence quenching by photoinduced electron transfer: a reporter for conformational dynamics of macromolecules. *ChemPhysChem.* 10:1389–1398. http://dx.doi.org/10.1002/cphc.200900238

Gandhi, C.S., and R. Olcese. 2008. The voltage-clamp fluorometry technique. *Methods Mol. Biol.* 491:213–231. http://dx.doi.org/10.1007/978-1-59745-526-8_17

Haug, T., D. Sigg, S. Ciani, L. Toro, E. Stefani, and R. Olcese. 2004. Regulation of K^+ flow by a ring of negative charges in the outer pore of BK_{Ca} channels. Part I. Aspartate 292 modulates K^+ conduction by external surface charge effect. *J. Gen. Physiol.* 124:173–184. http://dx.doi.org/10.1085/jgp.200308949

Horrigan, F.T., and R.W. Aldrich. 2002. Coupling between voltage sensor activation, Ca^{2+} binding and channel opening in large conductance (BK) potassium channels. *J. Gen. Physiol.* 120:267–305. http://dx.doi.org/10.1085/jgp.20028605

Horrigan, F.T., and Z. Ma. 2008. Mg^{2+} enhances voltage sensor/gate coupling in BK channels. *J. Gen. Physiol.* 131:13–32. http://dx.doi.org/10.1085/jgp.200709877

Hou, S., S.H. Heinemann, and T. Hoshi. 2009. Modulation of BKCa channel gating by endogenous signaling molecules. *Physiology (Bethesda).* 24:26–35. http://dx.doi.org/10.1152/physiol.00032.2008

Islas, L.D., and W.N. Zagotta. 2006. Short-range molecular rearrangements in ion channels detected by tryptophan quenching of bimane fluorescence. *J. Gen. Physiol.* 128:337–346. http://dx.doi.org/10.1085/jgp.200609556

Javaherian, A.D., T. Yusifov, A. Pantazis, S. Franklin, C.S. Gandhi, and R. Olcese. 2011. Metal-driven operation of the human large-conductance voltage- and Ca2+-dependent potassium channel (BK) gating ring apparatus. *J. Biol. Chem.* 286:20701–20709. http://dx.doi.org/10.1074/jbc.M111.235234

Jeffries, O., N. Geiger, I.C. Rowe, L. Tian, H. McClafferty, L. Chen, D. Bi, H.G. Knaus, P. Ruth, and M.J. Shipston. 2010. Palmitoylation of the S0-S1 linker regulates cell surface expression of voltage- and calcium-activated potassium (BK) channels. *J. Biol. Chem.* 285:33307–33314. http://dx.doi.org/10.1074/jbc.M110.153940

Koval, O.M., Y. Fan, and B.S. Rothberg. 2007. A role for the S0 transmembrane segment in voltage-dependent gating of BK channels. *J. Gen. Physiol.* 129:209–220. http://dx.doi.org/10.1085/jgp.200609662

Latorre, R., and S. Brauchi. 2006. Large conductance Ca2+-activated K+ (BK) channel: activation by Ca2+ and voltage. *Biol. Res.* 39:385–401. http://dx.doi.org/10.4067/S0716-97602006000300003

Latorre, R., and C. Miller. 1983. Conduction and selectivity in potassium channels. *J. Membr. Biol.* 71:11–30. http://dx.doi.org/10.1007/BF01870671

Latorre, R., F.J. Morera, and C. Zaelzer. 2010. Allosteric interactions and the modular nature of the voltage- and Ca2+-activated (BK) channel. *J. Physiol.* 588:3141–3148. http://dx.doi.org/10.1113/jphysiol.2010.191999

Lee, U.S., and J. Cui. 2010. BK channel activation: structural and functional insights. *Trends Neurosci.* 33:415–423. http://dx.doi.org/10.1016/j.tins.2010.06.004

Lee, U.S., J. Shi, and J. Cui. 2010. Modulation of BK channel gating by the β2 subunit involves both membrane-spanning and cytoplasmic domains of Slo1. *J. Neurosci.* 30:16170–16179. http://dx.doi.org/10.1523/JNEUROSCI.2323-10.2010

Liu, G., S.I. Zakharov, L. Yang, R.S. Wu, S.X. Deng, D.W. Landry, A. Karlin, and S.O. Marx. 2008. Locations of the beta1 transmembrane helices in the BK potassium channel. *Proc. Natl. Acad. Sci. USA.* 105:10727–10732. http://dx.doi.org/10.1073/pnas.0805212105

Liu, G., X. Niu, R.S. Wu, N. Chudasama, Y. Yao, X. Jin, R. Weinberg, S.I. Zakharov, H. Motoike, S.O. Marx, and A. Karlin. 2010. Location of modulatory β subunits in BK potassium channels. *J. Gen. Physiol.* 135:449–459. http://dx.doi.org/10.1085/jgp.201010417

Long, S.B., E.B. Campbell, and R. Mackinnon. 2005. Crystal structure of a mammalian voltage-dependent Shaker family K+ channel. *Science.* 309:897–903. http://dx.doi.org/10.1126/science.1116269

Long, S.B., X. Tao, E.B. Campbell, and R. MacKinnon. 2007. Atomic structure of a voltage-dependent K+ channel in a lipid membrane-like environment. *Nature.* 450:376–382. http://dx.doi.org/10.1038/nature06265

Lu, R., A. Alioua, Y. Kumar, M. Eghbali, E. Stefani, and L. Toro. 2006. MaxiK channel partners: physiological impact. *J. Physiol.* 570: 65–72. http://dx.doi.org/10.1113/jphysiol.2005.098913

Ma, Z., X.J. Lou, and F.T. Horrigan. 2006. Role of charged residues in the S1–S4 voltage sensor of BK channels. *J. Gen. Physiol.* 127:309–328. http://dx.doi.org/10.1085/jgp.200509421

Magleby, K.L. 2003. Gating mechanism of BK (Slo1) channels: so near, yet so far. *J. Gen. Physiol.* 121:81–96. http://dx.doi.org/10.1085/jgp.20028721

Mannuzzu, L.M., M.M. Moronne, and E.Y. Isacoff. 1996. Direct physical measure of conformational rearrangement underlying potassium channel gating. *Science.* 271:213–216. http://dx.doi.org/10.1126/science.271.5246.213

Mansoor, S.E., H.S. McHaourab, and D.L. Farrens. 2002. Mapping proximity within proteins using fluorescence spectroscopy. A study of T4 lysozyme showing that tryptophan residues quench bimane fluorescence. *Biochemistry.* 41:2475–2484. http://dx.doi.org/10.1021/bi011198i

Mansoor, S.E., M.A. Dewitt, and D.L. Farrens. 2010. Distance mapping in proteins using fluorescence spectroscopy: the tryptophan-induced quenching (TrIQ) method. *Biochemistry.* 49:9722–9731. http://dx.doi.org/10.1021/bi100907m

Meera, P., M. Wallner, M. Song, and L. Toro. 1997. Large conductance voltage- and calcium-dependent K+ channel, a distinct member

of voltage-dependent ion channels with seven N-terminal transmembrane segments (S0-S6), an extracellular N terminus, and an intracellular (S9-S10) C terminus. *Proc. Natl. Acad. Sci. USA.* 94:14066–14071. http://dx.doi.org/10.1073/pnas.94.25.14066

Morera, F.J., A. Alioua, P. Kundu, M. Salazar, C. Gonzales, A.D. Martinez, E. Stefani, L. Toro, and R. Latorre. 2012. The first transmembrane domain (TM1) of β2-subunit binds to the transmembrane domain S1 of α-subunit in BK potassium channels. *FEBS Lett.* In press.

Morrow, J.P., S.I. Zakharov, G. Liu, L. Yang, A.J. Sok, and S.O. Marx. 2006. Defining the BK channel domains required for beta1-subunit modulation. *Proc. Natl. Acad. Sci. USA.* 103:5096–5101. http://dx.doi.org/10.1073/pnas.0600907103

Nelson, R.D., G. Kuan, M.H. Saier Jr., and M. Montal. 1999. Modular assembly of voltage-gated channel proteins: a sequence analysis and phylogenetic study. *J. Mol. Microbiol. Biotechnol.* 1:281–287.

Orio, P., and R. Latorre. 2005. Differential effects of β1 and β2 subunits on BK channel activity. *J. Gen. Physiol.* 125:395–411. http://dx.doi.org/10.1085/jgp.200409236

Orio, P., P. Rojas, G. Ferreira, and R. Latorre. 2002. New disguises for an old channel: MaxiK channel beta-subunits. *News Physiol. Sci.* 17:156–161.

Pantazis, A., V. Gudzenko, N. Savalli, D. Sigg, and R. Olcese. 2010a. Operation of the voltage sensor of a human voltage- and Ca2+-activated K+ channel. *Proc. Natl. Acad. Sci. USA.* 107:4459–4464. http://dx.doi.org/10.1073/pnas.0911959107

Pantazis, A., A.P. Kohanteb, and R. Olcese. 2010b. Relative motion of transmembrane segments S0 and S4 during voltage sensor activation in the human BK_{Ca} channel. *J. Gen. Physiol.* 136:645–657. http://dx.doi.org/10.1085/jgp.201010503

Rothberg, B.S., and K.L. Magleby. 2000. Voltage and Ca^{2+} activation of single large-conductance Ca^{2+}-activated K^+ channels described by a two-tiered allosteric gating mechanism. *J. Gen. Physiol.* 116:75–99. http://dx.doi.org/10.1085/jgp.116.1.75

Salkoff, L., A. Butler, G. Ferreira, C. Santi, and A. Wei. 2006. High-conductance potassium channels of the SLO family. *Nat. Rev. Neurosci.* 7:921–931. http://dx.doi.org/10.1038/nrn1992

Savalli, N., A. Kondratiev, L. Toro, and R. Olcese. 2006. Voltage-dependent conformational changes in human Ca(2+)- and voltage-activated K(+) channel, revealed by voltage-clamp fluorometry. *Proc. Natl. Acad. Sci. USA.* 103:12619–12624. http://dx.doi.org/10.1073/pnas.0601176103

Savalli, N., A. Kondratiev, S.B. de Quintana, L. Toro, and R. Olcese. 2007. Modes of operation of the BKCa channel beta2 subunit. *J. Gen. Physiol.* 130:117–131. http://dx.doi.org/10.1085/jgp.200709803

Savalli, N., A. Pantazis, T. Yusifov, D. Sigg, and R. Olcese. 2012. The contribution of RCK domains to human BK channel allosteric activation. *J. Biol. Chem.* 287:21741–21750. http://dx.doi.org/10.1074/jbc.M112.346171

Schreiber, M., and L. Salkoff. 1997. A novel calcium-sensing domain in the BK channel. *Biophys. J.* 73:1355–1363. http://dx.doi.org/10.1016/S0006-3495(97)78168-2

Semenova, N.P., K. Abarca-Heidemann, E. Loranc, and B.S. Rothberg. 2009. Bimane fluorescence scanning suggests secondary structure near the S3-S4 linker of BK channels. *J. Biol. Chem.* 284:10684–10693. http://dx.doi.org/10.1074/jbc.M808891200

Shen, K.Z., A. Lagrutta, N.W. Davies, N.B. Standen, J.P. Adelman, and R.A. North. 1994. Tetraethylammonium block of Slowpoke calcium-activated potassium channels expressed in Xenopus oocytes: evidence for tetrameric channel formation. *Pflugers Arch.* 426:440–445. http://dx.doi.org/10.1007/BF00388308

Stefani, E., and F. Bezanilla. 1998. Cut-open oocyte voltage-clamp technique. *Methods Enzymol.* 293:300–318. http://dx.doi.org/10.1016/S0076-6879(98)93020-8

Stefani, E., M. Ottolia, F. Noceti, R. Olcese, M. Wallner, R. Latorre, and L. Toro. 1997. Voltage-controlled gating in a large conductance Ca2+-sensitive K+channel (hslo). *Proc. Natl. Acad. Sci. USA.* 94:5427–5431. http://dx.doi.org/10.1073/pnas.94.10.5427

Sun, X., M.A. Zaydman, and J. Cui. 2012. Regulation of voltage-activated K(+) channel gating by transmembrane β subunits. *Front Pharmacol.* 3:63.

Swartz, K.J. 2004. Towards a structural view of gating in potassium channels. *Nat. Rev. Neurosci.* 5:905–916. http://dx.doi.org/10.1038/nrn1559

Swartz, K.J. 2008. Sensing voltage across lipid membranes. *Nature.* 456:891–897. http://dx.doi.org/10.1038/nature07620

Sweet, T.B., and D.H. Cox. 2008. Measurements of the BK_{Ca} channel's high-affinity Ca^{2+} binding constants: effects of membrane voltage. *J. Gen. Physiol.* 132:491–505. http://dx.doi.org/10.1085/jgp.200810094

Tombola, F., M.M. Pathak, and E.Y. Isacoff. 2006. How does voltage open an ion channel? *Annu. Rev. Cell Dev. Biol.* 22:23–52. http://dx.doi.org/10.1146/annurev.cellbio.21.020404.145837

Toro, L., M. Wallner, P. Meera, and Y. Tanaka. 1998. Maxi-K(Ca), a unique member of the voltage-gated K channel superfamily. *News Physiol. Sci.* 13:112–117.

Unnerståle, S., J. Lind, E. Papadopoulos, and L. Mäler. 2009. Solution structure of the HsapBK K+ channel voltage-sensor paddle sequence. *Biochemistry.* 48:5813–5821. http://dx.doi.org/10.1021/bi9004599

Wallner, M., P. Meera, M. Ottolia, G.J. Kaczorowski, R. Latorre, M.L. Garcia, E. Stefani, and L. Toro. 1995. Characterization of and modulation by a beta-subunit of a human maxi KCa channel cloned from myometrium. *Receptors Channels.* 3:185–199.

Wallner, M., P. Meera, and L. Toro. 1996. Determinant for beta-subunit regulation in high-conductance voltage-activated and Ca(2+)-sensitive K+ channels: an additional transmembrane region at the N terminus. *Proc. Natl. Acad. Sci. USA.* 93:14922–14927. http://dx.doi.org/10.1073/pnas.93.25.14922

Wang, L., and F.J. Sigworth. 2009. Structure of the BK potassium channel in a lipid membrane from electron cryomicroscopy. *Nature.* 461:292–295. http://dx.doi.org/10.1038/nature08291

Wei, A., C. Solaro, C. Lingle, and L. Salkoff. 1994. Calcium sensitivity of BK-type KCa channels determined by a separable domain. *Neuron.* 13:671–681. http://dx.doi.org/10.1016/0896-6273(94)90034-5

Wu, R.S., and S.O. Marx. 2010. The BK potassium channel in the vascular smooth muscle and kidney: α- and β-subunits. *Kidney Int.* 78:963–974. http://dx.doi.org/10.1038/ki.2010.325

Wu, R.S., N. Chudasama, S.I. Zakharov, D. Doshi, H. Motoike, G. Liu, Y. Yao, X. Niu, S.X. Deng, D.W. Landry, et al. 2009. Location of the beta 4 transmembrane helices in the BK potassium channel. *J. Neurosci.* 29:8321–8328. http://dx.doi.org/10.1523/JNEUROSCI.6191-08.2009

Wu, Y., Y. Yang, S. Ye, and Y. Jiang. 2010. Structure of the gating ring from the human large-conductance Ca(2+)-gated K(+) channel. *Nature.* 466:393–397. http://dx.doi.org/10.1038/nature09252

Xia, X.M., X. Zeng, and C.J. Lingle. 2002. Multiple regulatory sites in large-conductance calcium-activated potassium channels. *Nature.* 418:880–884. http://dx.doi.org/10.1038/nature00956

Yang, H., J. Shi, G. Zhang, J. Yang, K. Delaloye, and J. Cui. 2008. Activation of Slo1 BK channels by Mg2+ coordinated between the voltage sensor and RCK1 domains. *Nat. Struct. Mol. Biol.* 15:1152–1159. http://dx.doi.org/10.1038/nsmb.1507

Yuan, P., M.D. Leonetti, A.R. Pico, Y. Hsiung, and R. MacKinnon. 2010. Structure of the human BK channel Ca2+-activation apparatus at 3.0 A resolution. *Science.* 329:182–186. http://dx.doi.org/10.1126/science.1190414

Yuan, P., M.D. Leonetti, Y. Hsiung, and R. MacKinnon. 2012. Open structure of the Ca2+ gating ring in the high-conductance Ca2+-activated K+ channel. *Nature.* 481:94–97. http://dx.doi.org/10.1038/nature10670

Yusifov, T., N. Savalli, C.S. Gandhi, M. Ottolia, and R. Olcese. 2008. The RCK2 domain of the human BKCa channel is a calcium sensor. *Proc. Natl. Acad. Sci. USA.* 105:376–381. http://dx.doi.org/10.1073/pnas.0705261105

Yusifov, T., A.D. Javaherian, A. Pantazis, C.S. Gandhi, and R. Olcese. 2010. The RCK1 domain of the human BK_{Ca} channel transduces Ca^{2+} binding into structural rearrangements. *J. Gen. Physiol.* 136: 189–202. http://dx.doi.org/10.1085/jgp.200910374

Zeng, X.H., X.M. Xia, and C.J. Lingle. 2005. Divalent cation sensitivity of BK channel activation supports the existence of three distinct binding sites. *J. Gen. Physiol.* 125:273–286. http://dx.doi.org/10.1085/jgp.200409239

Zhang, G., S.Y. Huang, J. Yang, J. Shi, X. Yang, A. Moller, X. Zou, and J. Cui. 2010. Ion sensing in the RCK1 domain of BK channels. *Proc. Natl. Acad. Sci. USA.* 107:18700–18705. http://dx.doi.org/10.1073/pnas.1010124107